Tool wear assessment and life prediction model based on image processing and deep learning

Cheng Wu
Shenlong Wang (shenlongwang@usst.edu.cn)
University of Shanghai for Science and Technology https://orcid.org/0000-0001-6670-4412

Research Article

Keywords: Drill bit wear, Wear assessment, Image processing, U-Net, Migration learning

Posted Date: October 7th, 2022

DOI: https://doi.org/10.21203/rs.3.rs-2111214/v1

Tool wear assessment and life prediction model based on image processing and deep learning

Cheng Wu, Shenlong Wang*

University of Shanghai for Science and Technology, Shanghai 200093, P. R. China

*Corresponding Author (e-mail: shenlongwang@usst.edu.cn)

Abstract In the machinery field, drilling is one of the most important machining methods. Real-time monitoring of drill wear can effectively prevent the part quality from not meeting the specifications due to drill failure. This paper proposes a tool wear assessment and life prediction model based on image processing and deep learning methods, which shows great performance for small sample datasets and for low quality images. We construct an image database of drill bits and extract the normal areas and worn areas of the drill bits using the U-Net network and traditional image processing methods, respectively. Moreover, the original dataset is classified using the migration learning technique. The wear level of a drill bit can be accurately evaluated through experimental tests. Testing results show that the proposed method is more convenient and efficient than the previous methods that used manual measurements; the results can be applied to real-time drill wear monitoring, thereby reducing part damage caused by tool wear.

Keywords: Drill bit wear; Wear assessment; Image processing; U-Net; Migration learning

1 Introduction

In the current industry 4.0 era, hole machining is currently one of the most crucial machining methods [1]. In aircraft machining, in particular, there are nearly 1.5 million connections on a modern large aircraft, which means that a large number of holes need to be drilled [2]. When drilling, with the rotation and feed movement of the tool, the surface temperature of the tool increases continuously, and the drill bit is prone to wear during this process. In the actual machining process, the conservative method is to replace the tool based on experience. This method will misjudge the wear condition of the tool in many cases and replace it when the tool still has a certain service life or when the tool has been severely worn. Replacement is not conducive to production efficiency improvements and product competitiveness. Therefore, the evaluation of the wear condition of the tool can provide a certain reference for the production personnel and effectively improve the quality of the machined parts.

At present, the image processing method is a noncontact method mainly used to detect tool wear conditions. It can extract the area of interest without contact, thus helping scholars to establish a series of wear characteristics. Zhou et al. [3] used image processing to obtain the worn area of a tool and improved the accuracy of the subpixel edge detection algorithm based on Zernike moments. Huang et al. [4] used image projection and edge detection algorithms to calculate tool geometry. Sukeri et al. [5] used an image preprocessing operation to obtain edge images of the drill bits and then compared worn to nonworn drill edges.

In the past few years, due to the development of hardware technology, machine learning technology has become one of the important methods of current research. Therefore, scholars have studied extracting features of the tool image to classify or regress the wear degree of the tool through

machine learning technology. Gu et al. [6] proposed inputting the wear features extracted from the preprocessed images into the support vector machine (SVM) to predict the wear degree of the drill bit. The literature [7] used the B-ORCHIZ shape-based feature descriptor and used SVM to classify the degree of tool wear. Some scholars also use deep learning algorithms to assist in evaluating the wear condition of the tool. Zhang et al. [8] used YOLOv3 to locate the defective part of the tool, and then used the traditional image processing method to evaluate the width and length of the tool defect.

In general, a tool wear assessment method mainly consists of two steps, feature extraction and wear degree classification or regression [9, 10]. These methods often have a good effect on a tool wear evaluation because they construct a perfect eigenvector to characterize the wear condition of the drill bit [11]. However, at the same time, the previous research also has some shortcomings. In the feature extraction part, these methods often require certain prior knowledge, and some algorithms cannot evaluate tools with complex defect shapes. In research using image processing methods when extracting the wear and nonworn areas of the tool, the background of the grayscale image needs to have a strong contrast with the target. For grayscale images with low contrast, threshold segmentation or edge detection algorithms cannot achieve effective results. Therefore, it is necessary to propose a method that can still extract the tool contour when the contrast between the tool background and the target is not high and establish a highly robust wear quality evaluation system.

In this paper we establish an automatic tool wear assessment and life prediction model. The main research contributions of this article are as follows: (1) We established an image dataset of drill wear, which is divided into six categories according to the number of holes drilled by the drill; (2) For the problem that the contrast between the foreground and background of the captured drill image is not obvious, the U-Net semantic segmentation network [12] is used to segment the nonworn area of the drill bit; (3) Aiming at the problem of overfitting caused by the convolutional neural network (CNN) on a small sample dataset, the transfer learning method is used to train and test the drill wear image dataset.

The remainder of this paper is organized as follows: Section 2 defines the experimental equipment and experimental process. Section 3 introduces the theoretical method of the tool wear assessment model and transfer learning model used in this paper. Section 4 conducts related experiments to verify the accuracy and reliability of the proposed method. Finally, Section 5 is the conclusion.

2 Image library of tool wear

2.1 Experimental equipment

The benchtop drilling machine for drilling is the Z516, the maximum drilling diameter is 16 mm, and the maximum spindle speed is 3100 rpm. The feed rate is kept as consistent as possible while drilling. The equipment used to take images of drill wear is shown in Fig. 1, which includes a light source, an industrial microscope and a laptop. The pixel size of the original image collected by the visual device is 1920×1080.

2.2 Experimental process

We use a bench-top drilling machine and 10 high-speed steel (HSS) drills with a diameter of 2.9 mm as the main tools for the experiment. The material to be drilled is mainly 20-gauge steel, and the feed required to drill a hole is 8 mm. We set the spindle speed of the bench drill to

700 rpm and keep the feed rate as consistent as possible during the drilling process. We use the number of holes drilled as a classification standard for the drill wear. The first category is new drills, the second category is 10 holes drilled, the third category is 20 holes drilled, and the fourth category is drilling 30 holes, the fifth category is drilling 40 holes and the sixth category is drilling 50 holes. Photos of drill bits corresponding to these six categories are shown in Fig. 2.

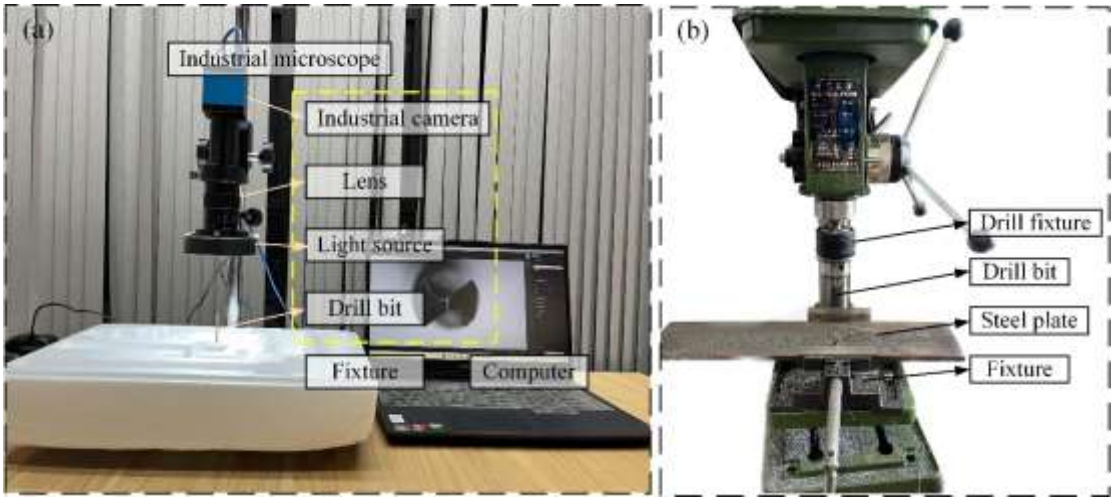

Fig. 1. Experimental setup used for obtaining tool wear images: (a) shooting equipment; (b) processing equipment.

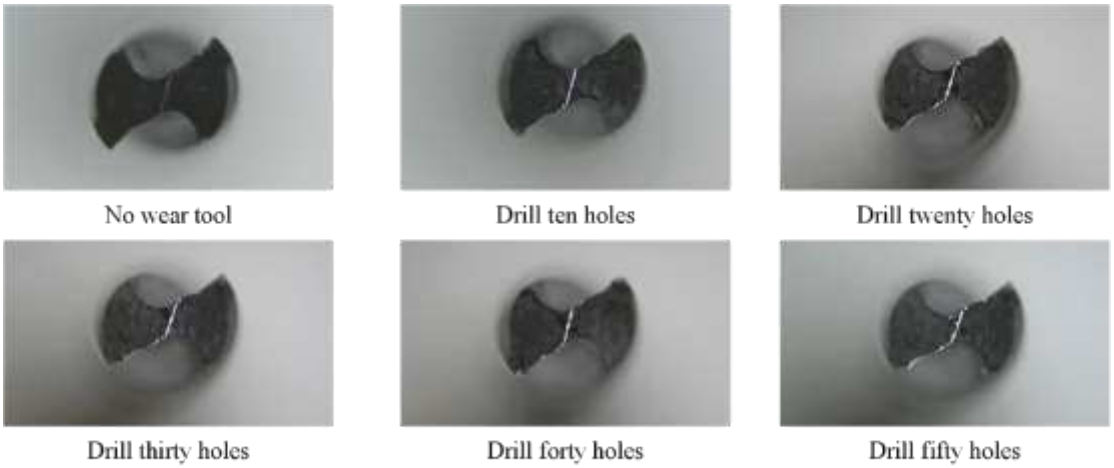

Fig. 2. Drill Wear Category Chart.

During the experiment, a fracture occurred when the drill bit reached the 57th hole. To be on the safe side, we define the drill to fail at 50 holes. Finally, we obtain a drill bit wear image dataset with 10 images per category. Each image corresponds to a drill bit, and a total of 60 images. When evaluating the wear condition of the tool, the nonworn area of the tool cannot be segmented by the traditional image processing method due to the unclear outline of the tool, therefore the U-Net network is used in this paper, and 35 belt parts are used in the literature. Annotated training images [12], 30 images consisting of 5 drills are used as the training set, and the remaining 30 images are used as the testing set. The distribution of the datasets is shown in Fig. 3(a), while Fig. 3(b) shows the distribution of the training and test sets for predicting bit life. The reason for the ratio being set as 8:2 will be discussed in Section 4.2.

3 Theoretical approach

Based on the collected tool wear image dataset, we first use the deep learning model to extract the tool surface contour. The worn areas are then extracted using image processing techniques. The intersection between these two binary images constitutes the final worn area. The flow chart of the wear evaluation method is shown in Fig. 4. Then, we apply transfer learning techniques to classify the extent of tool wear.

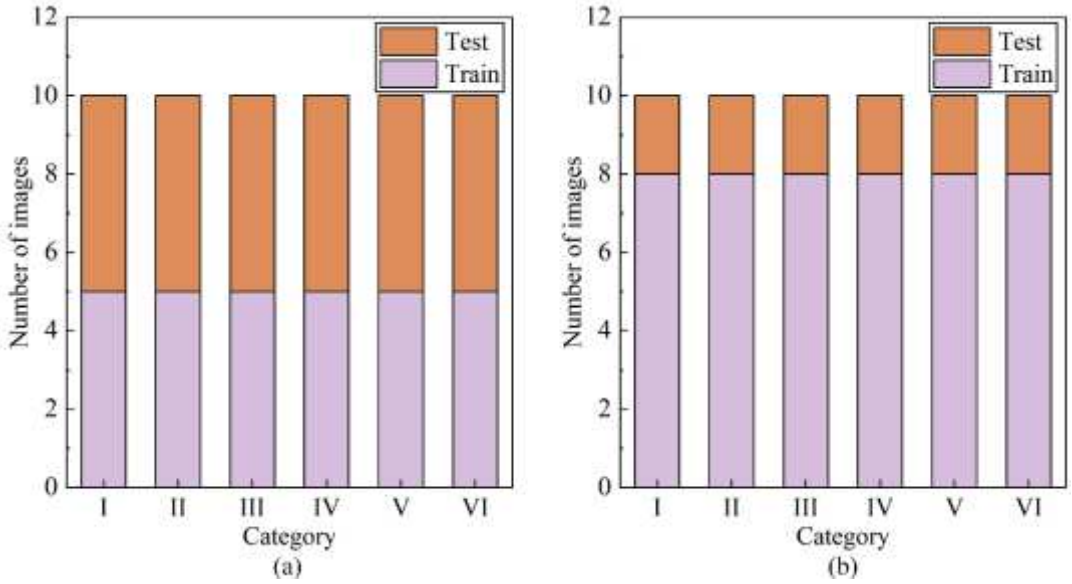

Fig. 3. Assignment of tool datasets: (a) tool wear evaluation model; (b) tool life prediction model.

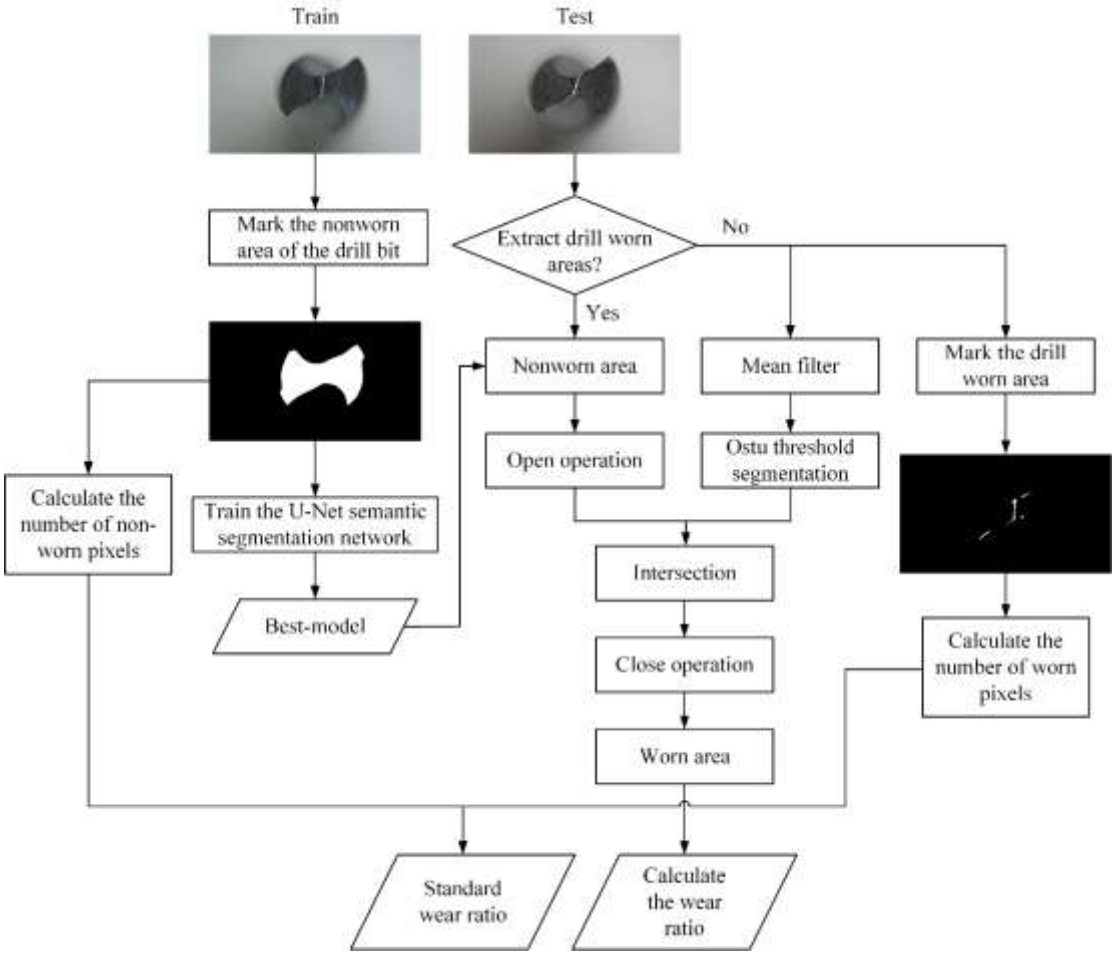

Fig. 4. Flow chart of the tool wear assessment method.

3.1 U-Net

Due to the influence of light and the shooting angle, the background and foreground areas of the obtained original image of the tool are not obvious. Therefore, it is difficult to segment the nonworn area of the tool using traditional processing methods. The classic image segmentation network U-Net is used in this study, which was originally designed for use in the medical field [13].

CNNs are widely used in many studies, such as VGG [14], GoogLeNet [15] and ResNet [16]. The last layer of the CNN is a fully connected layer, which compresses the feature map obtained by the original image through the convolution layer, pooling layer and activation function into a vector, and the output result is only the label of the image. Compared with CNN, U-Net is a pixel-level classification. The network is mainly composed of two parts, namely the feature extraction part and the upsampling part. The feature extraction part mainly uses the convolutional layer, the pooling layer, and the ReLU nonlinear activation function. The sampling part mainly uses the transposed convolution layer and the convolution layer.

As we only need to divide each pixel in the tool image into two categories, foreground and background, that is, the background and the nonworn area of the tool, the number of channels finally output by the network is 2, and the structure diagram of the network is shown in Fig. 5.

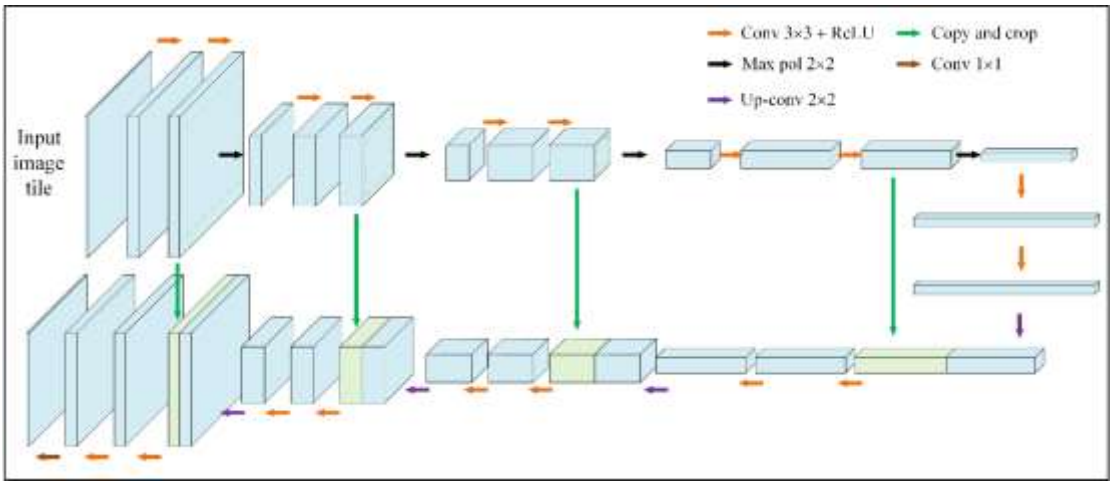

Fig. 5. U-Net structure diagram.

We use U-Net to segment the nonworn areas of the tool and end up with a binary image with only black and white colors. Since the edge of the binary image output by network segmentation has many sawtooth shapes, it is necessary to use an open operation to eliminate the image details smaller than the structural elements and smooth the image boundary [17]. The open operation is expressed as follows:

$$S \circ F = (S \ominus F) \oplus F \tag{1}$$

where S is a structure that can be set to different shapes. F is the set of foreground pixels. First, structural element F corrodes S, and then the result after the corrosion of structural element F expands.

Denote the binary image as $f(x, y)$, where (x, y) is a plane coordinate. The size of the image is $M \times N$. As the gray value of the binary image we obtained is not in the interval [0,1], we need to normalize the binary image, as shown in

$$fn(x, y) = \frac{f(x, y) - \min\limits_{0 \le x \le M, 0 \le y \le N} f(x, y)}{\max\limits_{0 \le x \le M, 0 \le y \le N} f(x, y) - \min\limits_{0 \le x \le M, 0 \le y \le N} f(x, y)} \tag{2}$$

After normalization, the gray value of the white area of the binary image is 1, and the gray value of the black area is 0, so we can count the number of pixels in the nonworn area of the tool. The number of pixels in the nonworn area of the tool is defined as

$$NON = \sum_{i=1}^{M} \sum_{j=1}^{N} fn(i, j) \tag{3}$$

3.2 Segmentation of tool worn area

Through the deep learning network U-Net, we can segment the nonworn area from the original tool image. Grayscale original tool images can convert the three-channel image into a one-channel image, the calculation amount can be reduced, and the computational efficiency can be effectively improved. The grayscale value of each pixel can be calculated by

$$g(x, y) = \alpha R + \beta G + \gamma B;\ x = 1, 2, 3...M \text{ and } y = 1, 2, 3...N \tag{4}$$

In Eq. (4), $g(x, y)$ represents the gray value of the image at point (x, y), and α, β and γ are all constants. According to the research, the values of the three are 0.2989, 0.5870 and 0.1140, respectively. R, G and B are the values at point (x, y) for each channel of the original tool image:

$$\begin{cases} R = F(x, y, 1) \\ G = F(x, y, 2) \\ B = F(x, y, 3) \end{cases} \tag{5}$$

In the process of acquiring the image, due to the sensor element or the external environment, the image transmitted to the computer usually has noise [18], so we use the mean filter to filter the grayscale tool, and the expression of the mean filter is shown follows:

$$h(x, y) = \frac{1}{pq} \sum_{(s,t) \in S_{xy}} g(s, t) \tag{6}$$

where $g(s, t)$ represents the grayscale image of the original image of the tool; $h(x, y)$ represents the filtered image of the grayscale image; S_{xy} represents the mean filter whose center is (x, y), and the size is $p \times q$; and s and t are the row and column coordinates of the pixel contained in the filter when the filter slides to the specified position.

After preprocessing, an appropriate threshold should be selected to classify the image at the pixel level. In this study, the wo area of the tool needs to be extracted using a threshold segmentation method, so only the pixels need to be assigned to two categories.

For grayscale images, an appropriate threshold can be selected by observing the grayscale histogram, as shown in Fig. 6. This method can always find a suitable threshold after many attempts for a single image, but for a large number of images, it will drastically increase our workload. The Otsu method is an adaptive threshold segmentation method [19], that is completely based on the histogram of the image, and separates an optimal threshold according to the gray value to segment the image into two parts, the background and target. Using {0,1,2...Q-1} to represent the Q gray levels in the image, by selecting the threshold t, the input image is divided into two categories, C1 and C2. The gray pixel value of category C1 is in the range of [0, t], and the gray pixel value of category C2 is in within the range [t+1, Q-1].

By counting the gray value of the gray image of the tool, let n_i represent the number of pixels

of gray level *i*, so we can normalize the histogram:

$$P_i = \frac{n_i}{\sum_{0}^{Q-1} n_i}, 0 \le p_i \le 1 \tag{7}$$

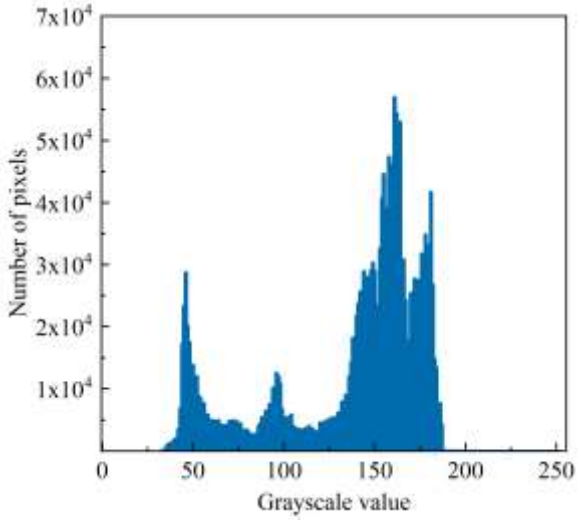

Fig. 6. Grayscale histogram.

The between-class variance can be expressed by

$$\sigma_B^2(t) = \frac{[m_G P_1(t) - m(t)]^2}{P_1(t)[1 - P_1(t)]} \tag{8}$$

where m_G is the average grayscale of the image, which can be represented by Eq. (9); $m(t)$ is the cumulative average value when the threshold is *t*, expressed by Eq. (10); the probability that an image pixel is assigned to class C1 can be represented by $P_1(t)$, represented by Eq. (11).

$$m_G = \sum_{i=0}^{Q-1} i p_i \tag{9}$$

$$m(t) = \sum_{i=0}^{t} i p_i \tag{10}$$

$$P_1(t) = \sum_{i=0}^{t} p_i \tag{11}$$

Our purpose is to find an optimal threshold $\hat{k}$ that maximizes the interclass variance:

$$\sigma_B^2(\hat{t}) = \max_{0 \le t \le Q-1} \sigma_B^2(t) \tag{12}$$

then, we can segment the grayscale image by a global threshold $\hat{k}$:

$$w(x,y) = \begin{cases} 0, & h(x,y) < \hat{k} \\ 1, & h(x,y) \ge \hat{k} \end{cases} \tag{13}$$

Due to the very high temperature during tool drilling, the tool may undergo plastic deformation. After the tool undergoes plastic deformation, we obtain the worn area through the Otsu threshold segmentation method[20], which will also segment this part of the area, which is obviously unreasonable. Thus, we use the nonworn area of the tool extracted in Section 2.2 and the area obtained by the Otsu threshold segmentation to take the intersection:

$$W = w\,\mathrm{I}\;\; fn \tag{14}$$

The preliminary tool wear image can be obtained by the Eq. (14). However, the extracted wear image has the problem of holes in the center and rough edges. Therefore, the closed operation is used to process the preliminary obtained binary image of tool wear, which can be expressed by

$$S \bullet F = (S \oplus F)\,\mathrm{e}\;\; F \tag{15}$$

After the closing operation, we can obtain the final binary image of the nonworn area of the tool. Similarly, we use Eq. (2) and Eq. (3) to count the number of pixels in the worn area of the tool and record the number of pixels in the worn area of the tool as WEA.

3.3 Transfer learning model

As it is very difficult to obtain image datasets with large sample sizes in the mechanical field [21, 22], for datasets with small sample sizes, directly using CNNs without initial weights to train small datasets will result in overfitting. However, transfer learning can first train a network on a large dataset, such as ImageNet [23]. Then, the pretrained model is used to train the small-sample dataset. There are already initial weights in the pretrained model when training the small-sample dataset, which can help us to fit more easily.

In this paper, we use the ResNet18 deep learning model [16] after pretraining on the large dataset ImageNet [23] to tune a hyperparameter to train our tool wear dataset. The transfer learning method is shown in Fig. 7.

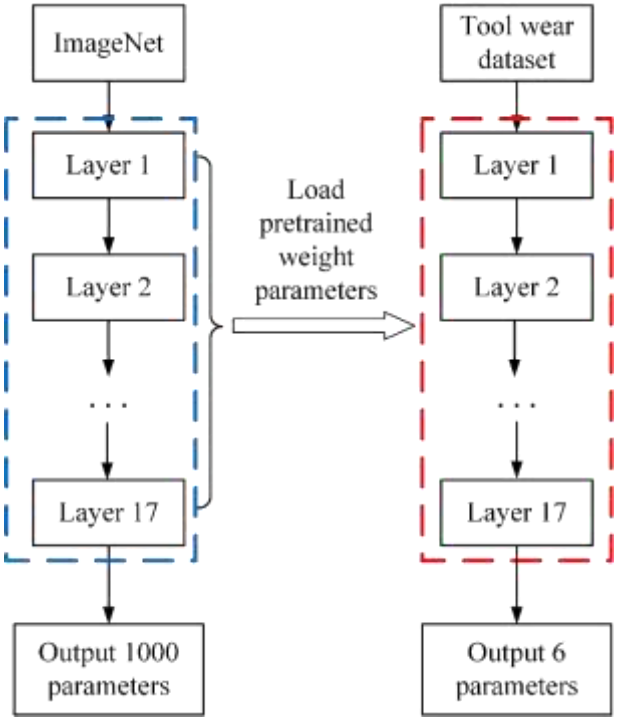

Fig. 7. Transfer learning model.

4 Experiments and Results

To verify the accuracy of the model, we conducted experiments to test its accuracy. First, industrial microscopes and computer equipment are used to collect the original tool image. Then, deep learning methods are used to preliminarily segment the nonworn area of the tool. Moreover,

the tool image is processed by a computer using the method proposed in this paper to obtain the worn and nonworn areas. The hardware and software equipment for training U-Net are shown in Table 1. At the same time, to attain a tool life prediction, we study the influence of different proportions of the training set and testing set and use different deep learning models for an accuracy of life prediction.

Table 1. Experimental environment

Name	Type
CPU	AMD R5 4600H
GPU	NVIDIA GeForce GTX1650
Python	3.6.13
Pytorch	1.10.1
CUDA	11.1.114

4.1 Validation of the Tool Wear Evaluation Model

The nonworn area of the tool is segmented by a pre-trained U-Net. For the worn area of the tool, traditional image processing methods can be used to extract the region of interest (ROI). The image processing process is shown in Fig. 8. All image processing operations are performed on MATLAB 2021b.

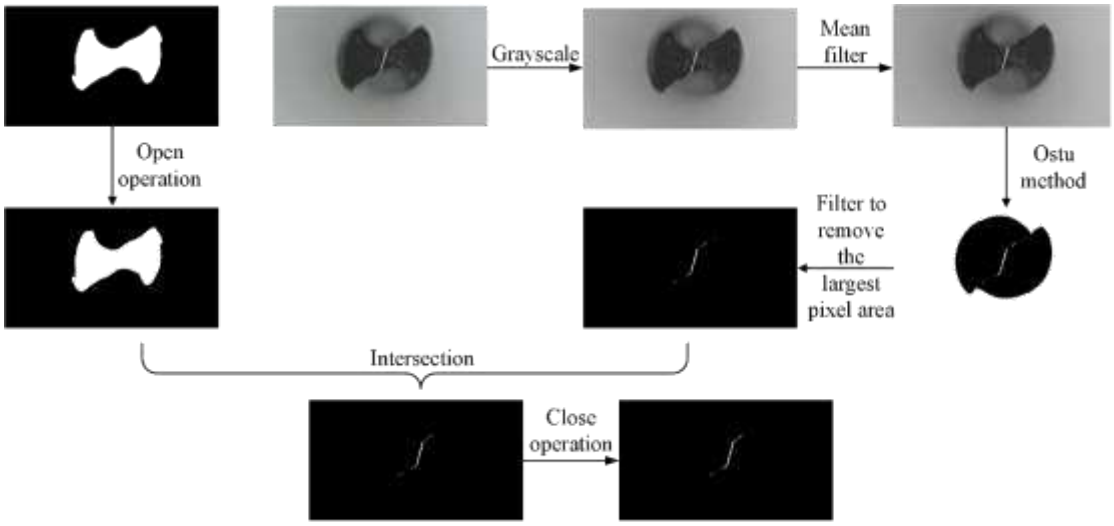

Fig. 8. Image processing.

To reflect the wear status of the tool, it is essential to calculate the ratio of the tool worn area to the entire tool area. The number of pixels in the worn area of the tool and the number of pixels in the nonworn area can be counted separately, as shown in Fig. 9. Since 5 drills are used for testing, and each drill drilled 10 holes to take a set of photos, 30 images are considered as the testing set.

The wear rate can be calculated based on the number of pixels in the tool wear and nonworn areas according to

$$\eta = \frac{WEA}{NON} \times 100\% \tag{16}$$

To compare the wear ratios obtained by the manual annotation method for two of the tools with the wear ratios obtained by the proposed method in this paper, we set the abscissa as the number of drilled holes and the ordinate as the tool wear ratio and draw the dot-line graph of the change in the tool wear ratio with the increase in the number of holes, as shown in Fig. 10. The comparison of the

wear ratio obtained by manual measurement with the wear ratio obtained by the proposed method in this paper is shown in Fig. 11, where the abscissa is the number of tools, a total of 5 tools are used for experimental testing, and the ordinate is the wear ratio.

To evaluate the error between the manual measurement and the experimental measurement of the wear ratio, the error is defined as Eq. (17).

$$\text{error} = \frac{|\eta_{test} - \eta_{label}|}{\eta_{label}} \times 100\% \tag{17}$$

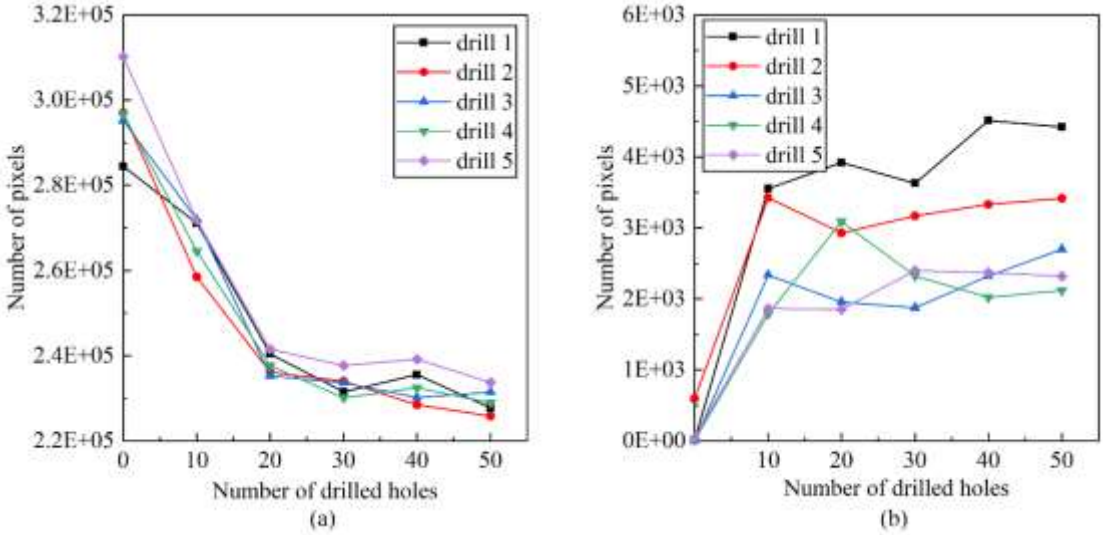

Fig. 9. Counts of the number of pixels of ROI in an image: (a) the number of pixels in the nonworn area of the tool; (b) the number of pixels in the tool worn area.

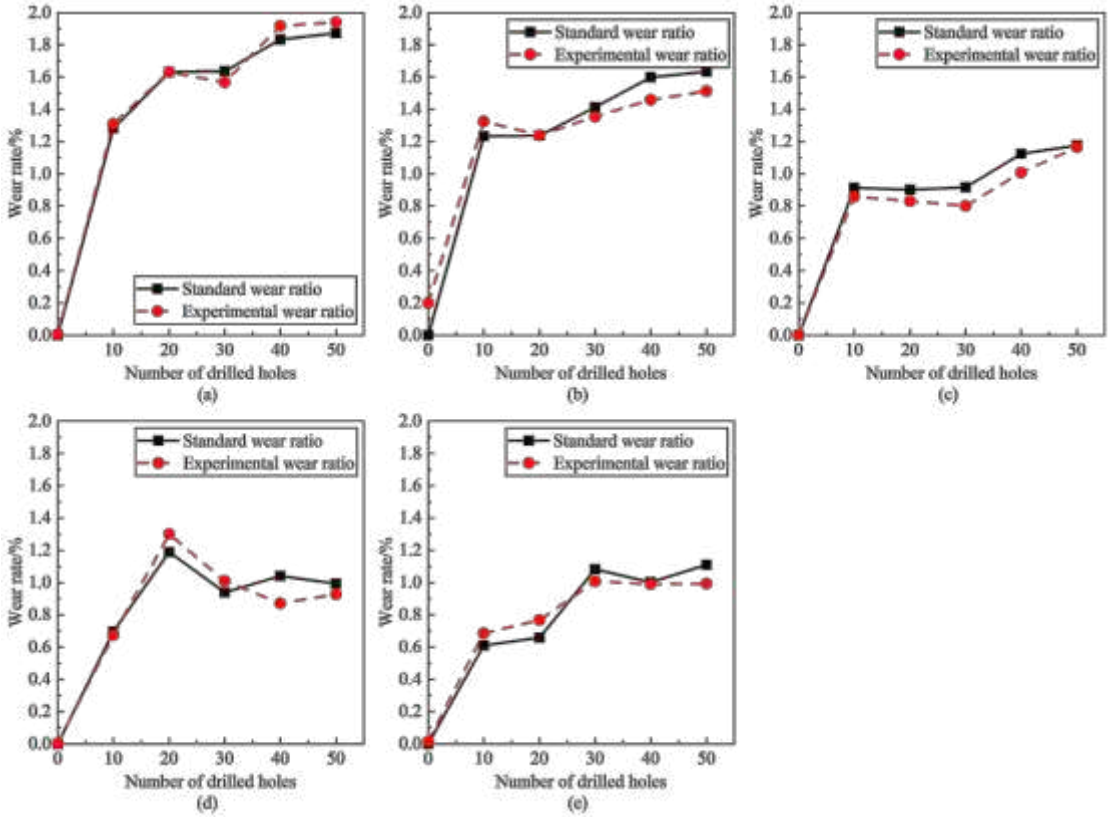

Fig. 10. Line chart of the results of the two measurement methods: (a) the first test drill; (b) the second test drill; (c) the third test drill; (d) the fourth test drill; (e) the fifth test drill.

where η_{test} is the wear ratio using the tool wear assessment method and η_{label} is the wear ratio using the manual measurement method.

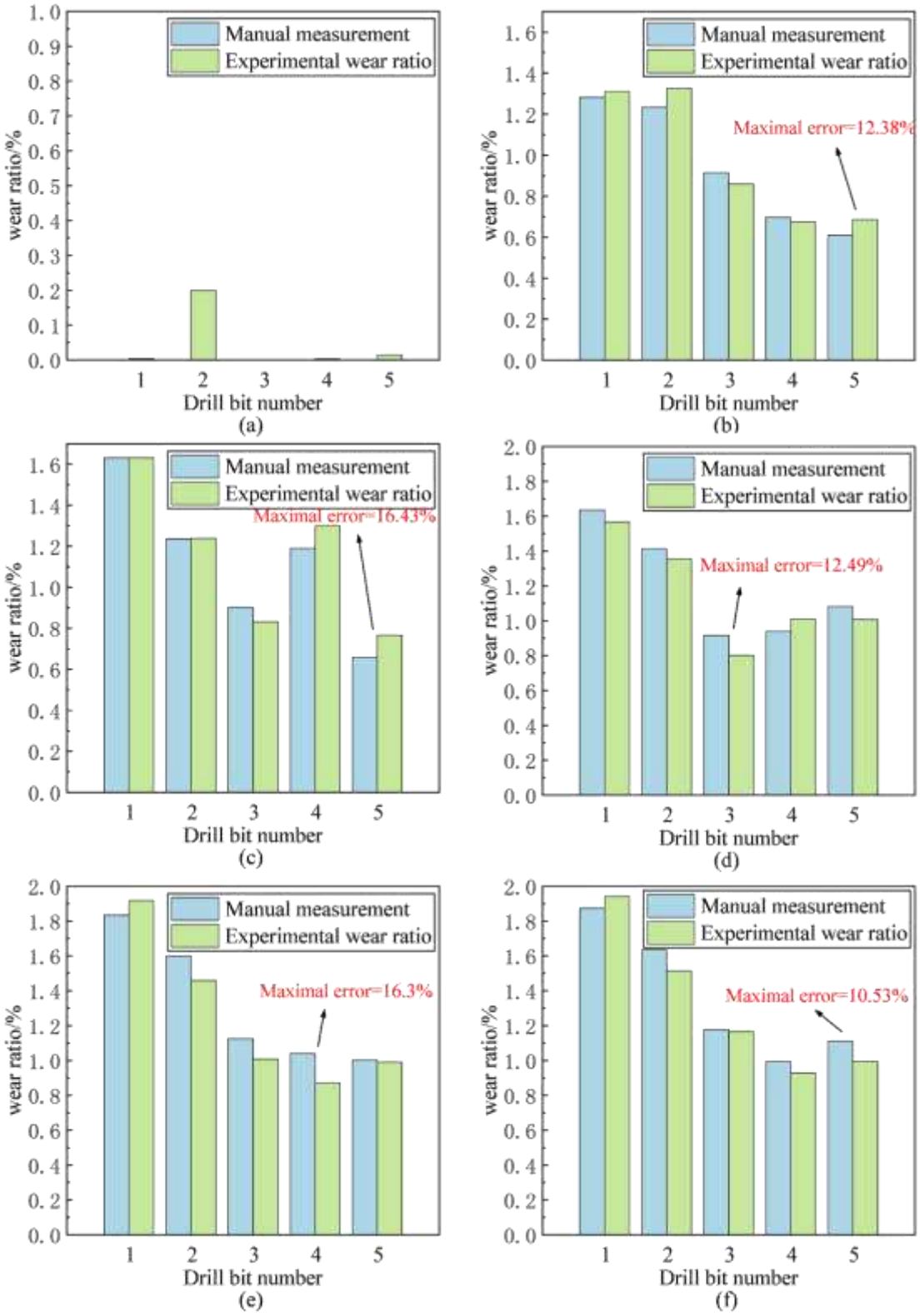

Fig. 11. Histogram of two measurement methods: (a) no drilling; (b) ten drilled holes; (c)twenty drilled holes; (d) thirty drilled holes; (e) forty drilled holes; (f) fifty drilled holes.

A maximum error of 16% between the experimental and manual measurements can be observed through the tool wear evaluation model experiment. There are 76% of the sample errors less than 10% and 40% of the sample errors less than 5%.

4.2 Validation of the transfer learning model

In the life prediction step, the transfer learning model is established to classify the wear degree of the tool to attain a life prediction of the tool. Transfer learning training is easier than directly training a new deep learning model because it uses a pretrained weight model [24, 25]. A deep learning model from ten years ago usually increased the number of network layers, while the more modern ResNet uses a residual structure to fuse the shallow features of the network with the deep features, which greatly improves the accuracy of image classification.

Given the small sample size of the tool wear dataset constructed in this paper, the ResNet18 network is used, as a ResNet with more layers will be more difficult to train and prone to overfitting. The main settings for training the transferred residual network are shown in Table 2. Moreover, data augmentation methods such as horizontal zoom, vertical zoom, reflection and translation are used.

Table 2. Experimental environment

Name	Type
Batch size	32
Epoch	200
Learning rate	10^{-3}
Momentum	0.9
Optimizer	SGDM

The R ratio of the training set and testing set is set to 9:1, 8:2, 7:3, 6:4, and 5:5 in the experiment. The experimental results obtained are shown in Fig. 12. It can be seen from the results that when the ratio is selected as 9:1, the highest accuracy is obtained in the experiment the most times, but the fluctuation is large, and the accuracy of one experiment decreases below 70%. When the ratio is selected as 8:2, although the number of times that the highest accuracy is obtained in the experiment is few, the result is relatively stable, and the average accuracy of 10 experiments can reach 91.67%, which is more than 90%.

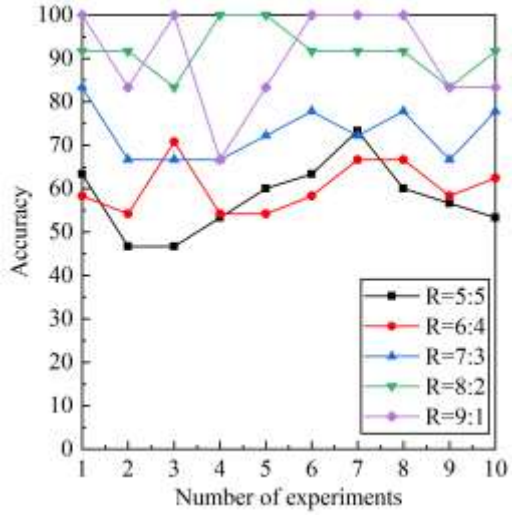

Fig. 12. Assign different weights to the training set and the testing set.

In image classification problems, using classification accuracy alone does not fully reflect the

effect of the deep learning models. Therefore, the confusion matrix is used to further evaluate the performance of the model. The confusion matrix is a $n \times n$ matrix, where n represents the number of categories of the classification, the elements on the diagonal of the matrix represent the number of correct predictions, and the elements on Row i and Column j represent the correct category but classify it as j. For the case where the proportion of the training set is 0.8, we obtain a confusion matrix diagram through several experiments, as shown in Fig. 13. It can be seen that the errors are mainly concentrated in the middle categories. The average classification accuracy exceeds 90%, and the minimum classification accuracy is also higher than 80%. Through experimental comparative research, it can be asserted that the migration model used in this paper accurately and effectively predicts tool life.

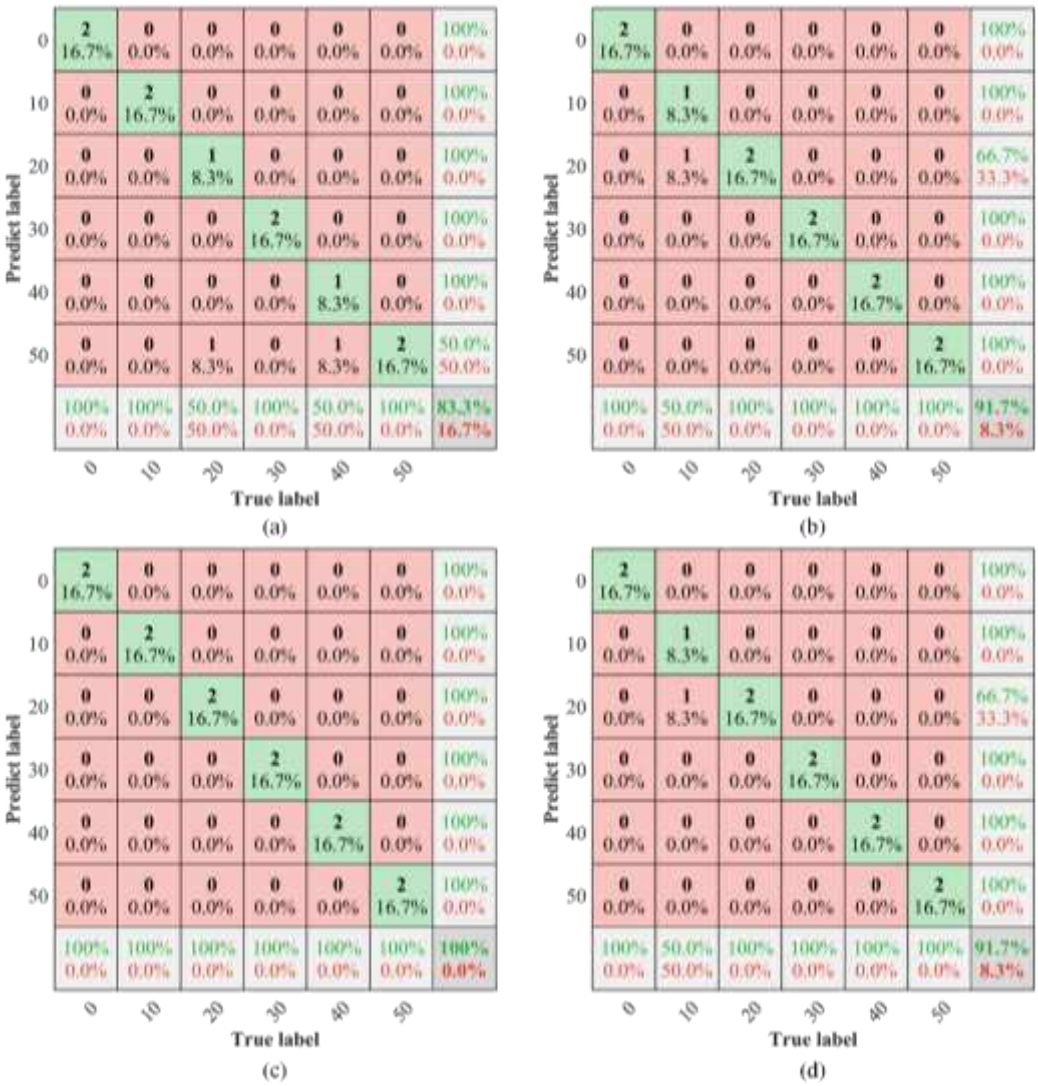

Fig. 13. Tool wear image classification results.

5 Conclusions

This article presents a novel tool wear assessment and life prediction method. First, the full contour of the tool is segmented using the semantic segmentation network U-Net. For the worn area in the tool, the Otsu threshold segmentation and morphological image processing methods were used. The transfer of the pretrained residual network helps us predict the number of holes that can

be made by the tool, thereby indirectly attaining a life prediction of the tool. The wear ratio calculated by the ratio of the extracted two parts of the tool is no more than 17% different from the manual measurement, and the error of more than half of the samples is no more than 10%. The tool life prediction model also has high accuracy, with an average accuracy of over 90%.

Based on the above characteristics of the tool wear assessment and life prediction model, we conclude that the proposed method can be used in real-time monitoring of machining tools. However, there are still some limitations in this study. On the one hand, the shooting angle, brightness of the surrounding environment and outside temperature still need to be considered in the model. On the other hand, the plastic deformation of the tool affects the accuracy of extracting the worn area. Therefore, it is necessary to develop a more general and robust model. We will report these studies in future publications.

Author contribution Cheng Wu: Conceptualization, Methodology, Code, Writing – original draft. Shenlong Wang: Conceptualization, Supervision, Funding acquisition, Writing – review & editing.

Funding The work is supported by the National Natural Science Foundation of China (Grant No. 12172226).

Availability of data and material Not applicable.

Code availability The authors confirm that the code supporting the findings of this work is available from the corresponding author upon reasonable request.

Declarations

Ethics approval The authors declare the compliance with the ethical standards.

Consent to participate All authors consent to participate.

Consent to publication All authors consent to publish.

Conflict of interest The authors declare that they have no conflicts of interest.

References

1. Parenti P, Pagani L and Annoni M. Automatic identification of edge chipping defects in high precision drilling of cemented carbide. *Precision Engineering-Journal of the International Societies for Precision Engineering and Nanotechnology* 2019; 60: 383-393.
2. Li GH, Yang S, Cao SM, et al. A semi-supervised deep learning approach for circular hole detection on composite parts. *Visual Computer* 2021; 37: 433-445.
3. Zhou J and Yu J. Chisel edge wear measurement of high-speed steel twist drills based on machine vision. *Computers in Industry* 2021; 128: 103436.
4. Huang CK, Liao CW, Huang AP, et al. An automatic optical inspection of drill point defects for micro-drilling. *International Journal of Advanced Manufacturing Technology* 2008; 37: 1133-1145.
5. Sukeri M, Paiz Ismadi MZ, Othman AR, et al. Wear Detection of Drill Bit by Image-based Technique. *IOP Conference Series: Materials Science and Engineering* 2018; 328.
6. Gu P, Zhu CM, Yu YQ, et al. Evaluation and prediction of drilling wear based on machine vision. *International Journal of Advanced Manufacturing Technology* 2021; 114: 2055-2074.
7. Garcia-Ordas MT, Alegre E, Gonzalez-Castro V, et al. A computer vision approach to analyze and classify tool wear level in milling processes using shape descriptors and machine learning techniques. *International Journal of Advanced Manufacturing Technology* 2017; 90: 1947-1961.
8. Zhang T, Zhang C, Wang Y, et al. A vision-based fusion method for defect detection of milling cutter

spiral cutting edge. *Measurement* 2021; 177: 109248.
9. Yang YT, Zheng HL, Li YB, et al. A fault diagnosis scheme for rotating machinery using hierarchical symbolic analysis and convolutional neural network. *Isa Transactions* 2019; 91: 235-252.
10. Worden K, Staszewski WJ and Hensman JJ. Natural computing for mechanical systems research: A tutorial overview. *Mechanical Systems and Signal Processing* 2011; 25: 4-111.
11. Hegab H, Hassan M, Rawat S, et al. A smart tool wear prediction model in drilling of woven composites. *The International Journal of Advanced Manufacturing Technology* 2020; 110: 2881-2892.
12. Ronneberger O, Fischer P and Brox T. U-Net: Convolutional Networks for Biomedical Image Segmentation. In: *International Conference on Medical Image Computing and Computer-Assisted Intervention* 2015: 234-241.
13. Wang ZW, Qin Y and Chen WW. Vision measurement of gear pitting based on DCGAN and U-Net. *Journal of Mechanical Science and Technology* 2021; 35: 2771-2779.
14. Simonyan K and Zisserman A. Very Deep Convolutional Networks for Large-Scale Image Recognition. *Computer Science* 2014.
15. Szegedy C, Liu W, Jia Y, et al. Going Deeper with Convolutions. In: 2015 *IEEE Conference on Computer Vision and Pattern Recognition* (*CVPR*) 2015: 1-9.
16. He K, Zhang X, Ren S, et al. Deep Residual Learning for Image Recognition. In: 2016 *IEEE Conference on Computer Vision and Pattern Recognition* (*CVPR*) 2016: 770-778.
17. He Y, Zhang W, Li Y-F, et al. An approach for surface roughness measurement of helical gears based on image segmentation of region of interest. *Measurement* 2021; 183: 109905.
18. Yugander P, Tejaswini CH, Meenakshi J, et al. MR Image Enhancement using Adaptive Weighted Mean Filtering and Homomorphic Filtering. *Procedia Computer Science* 2020; 167: 677-685.
19. He ZY, Yuan SY, Zhao JH, et al. A novel myocardial infarction localization method using multi-branch DenseNet and spatial matching-based active semi-supervised learning. *Information Sciences* 2022; 606: 649-668.
20. Otsu N. A threshold selection method from gray-level histograms. *IEEE Transactions on Systems, Man and Cybernetics* 1979; SMC-9: 62-66.
21. Li X, Zhang W and Ding Q. Cross-Domain Fault Diagnosis of Rolling Element Bearings Using Deep Generative Neural Networks. *IEEE Transactions on Industrial Electronics* 2019; 66: 5525-5534.
22. Kuang J, Xu G, Tao T, et al. Class-Imbalance Adversarial Transfer Learning Network for Cross-Domain Fault Diagnosis With Imbalanced Data. *IEEE Transactions on Instrumentation and Measurement* 2022; 71: 1-11.
23. Krizhevsky A, Sutskever I and Hinton GE. Imagenet classification with deep convolutional neural networks. *Advances in neural information processing systems* 2012; 25.
24. Zhuang FZ, Qi ZY, Duan KY, et al. A Comprehensive Survey on Transfer Learning. *Proceedings of the Ieee* 2021; 109: 43-76.
25. Fernandes K and Cardoso JS. Hypothesis transfer learning based on structural model similarity. *Neural Computing and Applications* 2019; 31: 3417-3430.